A Novel Robotic Meshworm With Segment-Bending Anchoring for Colonoscopy

Julius E. Bernth, *Student Member, IEEE*, Alberto Arezzo, and Hongbin Liu, *Member, IEEE*

***Abstract*—This letter introduces the design and evaluation of a novel worm-inspired, multisegment robotic endoscope with multiple degrees of freedom segments. The novelty of this design is that the robot is able to drive forwards and backwards, anchor itself, steer while inside a tubular structure and control the orientation of an end-mounted camera all by bending its flexible segments. The mechanical design is shown and a sensing system based on Hall Effect sensors is incorporated. In a simulated colon, a top speed of 1.21 mm/s was achieved, equivalent to roughly 38% of the theoretical maximum. These results are discussed and further improvements are suggested, followed by general concluding remarks.**

***Index Terms*—Biologically-inspired robots, medical robots and systems, soft material robotics.**

I. Introduction

COLORECTAL cancer accounts for approximately 10% of all known cancer cases worldwide and is therefore a serious cost to health services [1]. There is evidence to suggest that fear of discomfort is a significant reason for patients not attending regular bowel screenings [1]. As regular screenings are one of the best and most effective methods of preventing bowel cancer [2], the fact that only a little over half of the patients eligible for screening refuse to undergo colonoscopy impairs the effort of screening programs [2]. Finding a more comfortable alternative to traditional push endoscopes could significantly increase participation in regular pre-screenings. Worm-like robots present exactly such an alternative to push endoscopes and research towards improving worm-like robotic endoscope design could have significant impact on people's health and wellbeing. This letter will present a novel design for a soft, multi-segment worm robot.

Recently, a number of worm-like robots have been proposed. An early mesh-based robot consisted of three pneumatically actuated segments specifically intended for use in colonoscopy [3]. Bladder structures based on artificial muscles were inflated to cause an expansion and contraction in a particular segment. Doing this in proper sequence, peristaltic motion was achieved. The device was tested in a rigid plastic pipe to approximate a human intestine and achieved speeds of 5 mm/s. Menciassi *et al.* produced a device in [4] and [5] that relied on shape memory alloy (SMA) actuators to produce worm-like crawling motion. To ensure that the device would move forward, small hooks were embedded on the outer skin of the robot to increase friction in one direction. While effective during forward movement, this feature does, however, prevent the device from moving backwards. Designs presented in [6] and [7] rely on geared DC motors to actuate linkages between segments, thus producing peristaltic motion. Additionally, an anchoring mechanism was incorporated in the system presented in [6] which allows either the front-most or rear-most segment to increase friction on its surrounding environment. This anchoring mechanism was controllable and the device was able to move both forward and backward. The design presented in [8] consists of a spring-like, soft mesh which is then deformed by a series of SMA actuators. The arrangement of the actuators is inspired by how circular and longitudinal muscle fibres function in common earth worms. Motion is achieved through peristalsis. Additionally, a sensing system was employed to achieve position feedback control of each segment.

A number of commercial alternatives to the traditional endoscope exist. These include the Aeroscope [9], Invendoscope [10], [11], NeoGuide [12], [13] and Endotics Systems [14]. With regard to propulsion method, only Endotics uses an on-board, worm-inspired locomotion system. The Endotics system relies on a technique involving suction and clamping of local colon tissue to anchor either of its two end points. First, the front segment is anchored using suction and clamping. The central segment is then contracted to bring the rear segment forward, where after the rear segment is anchored. The middle segment is then extended and the sequence repeated, driving the device forward, similar to how an inchworm moves. The front segment, equipped with a camera and biopsy tool is able to orient the end segment.

In general, the above research prototypes use segments that have a single degree-of-freedom (DOF). Given that it is necessary to have control of camera orientation and steering in endoscopy, a single DOF system will not be sufficient. The commercial designs (for the most part) allow for camera orientation and steering. All but Endotics rely on force being applied externally to the colon in order to propel the endoscope.

Manuscript received September 9, 2016; accepted February 13, 2017. Date of publication March 6, 2017; date of current version May 16, 2017. This paper was recommended for publication by Associate Editor H. Liao and Editor A. Bicchi upon evaluation of the reviewers' comments. This work was supported by the EPSRC under Grant EP/N508986/1. *(Corresponding author: Hongbin Liu.)*

J. E. Bernth and H. Liu are with the Centre for Robotic Research (CoRe), Department of Informatics, King's College London, London WC2R 2LS, U.K. (e-mail: julius.bernth@kcl.ac.uk; hongbin.liu@kcl.ac.uk).

A. Arezzo is with the Department of Surgical Sciences, University of Turin, 10126 Turin, Italy (e-mail: alberto.arezzo@mac.com).

This letter has supplementary downloadable material available at http:// ieeexplore.ieee.org, provided by the authors.

Digital Object Identifier 10.1109/LRA.2017.2678540

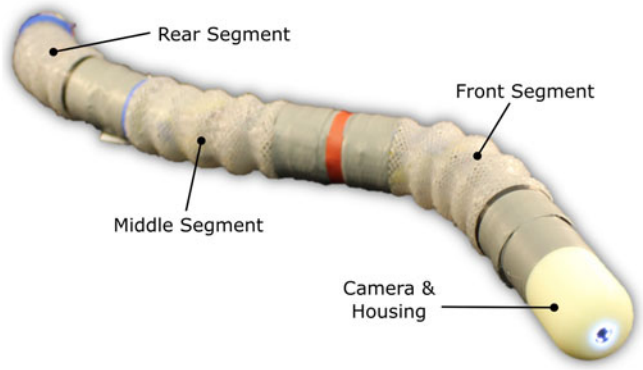

Fig. 1. Assembled prototype with an endoscopic camera mounted on the end of the device.

The Endotics design uses two separate mechanisms for anchoring and camera orientation/steering. The advantage of the design proposed in this letter is that it uses only one mechanism to achieve both anchoring and camera orientation/steering. Therefore, the complexity of the design is reduced relative to Endotics. Given that endoscopes are required to be very small in diameter, a reduction in complexity can lead to an increase in reliability. Additionally, this device is able to adapt to a varying colon diameter through use of the bending-anchoring method.

II. Design

A. Overview

The robot (see Fig. 1) consists of three separate segments. Each segment consists of an elastic mesh structure which is antagonistically driven by tendons. The tendons are wound around pulleys which are mounted on DC motors. As the motors rotate, the lengths of the tendons change, either compressing or extending the mesh body. Contraction of each segment is achieved by shortening a tendon, thus actively pulling the mesh. Extension is achieved by giving the tendons slack and allowing the mesh to passively expand due to its natural elasticity. The front and rear segments are actuated by three motors. Therefore, they have one linear DOF to accomplish contraction and extension and two rotational DOFs allowing bending about two axes. The middle segment only has a single, linear DOF for contraction and extension. The design is modular – segments can be fitted together in any order and motor housings can be swapped between meshes at will. With this in mind, the fundamental structure of any given segment is the same. This basic structure is shown in Fig. 2.

In order to evaluate the system's ability to function as an endoscope, a miniature USB camera (6 mm diameter, 640 × 480 resolution) with illuminating LEDs was mounted on the end of the prototype. The final prototype was approximately 50 cm in length. The camera cables were passed through the drive assemblies using specially designed passages (see Fig. 3). The sizes of these passages can be easily increased in the future. The camera is fixed in a plastic housing, attached at the tip of the front segment, where it would be possible in the future to mount additional equipment such as a biopsy tool.

The body of the robot is comprised of the polyethylene terephthalate (PET) mesh material proposed in [15]. The mesh has been heat treated around a specially designed mould, creating a ribbed structure. The flexible section of each mesh is approximately 80 mm long and has a stiffness equal to 0.223 N/mm over a strain range between 0 to 50%, which was sufficient for this design. The outer mesh could be made water tight and disposable to ensure sterilisation, allowing the drive assemblies to be reused with minimal cleaning and sterilisation effort.

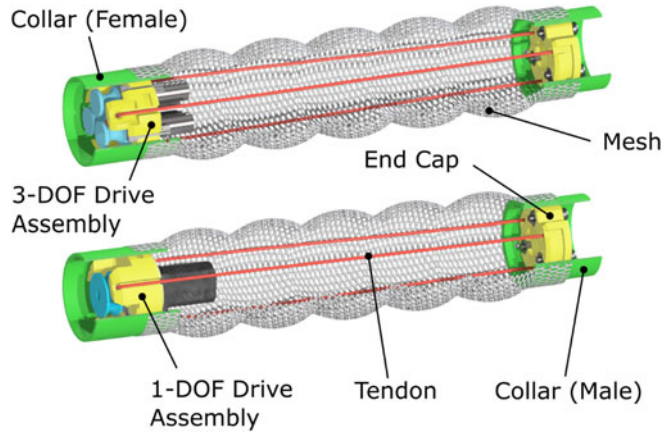

Fig. 2. Cut-away sections of computer models of the 3-DOF segment (top) and the 1-DOF segment (bottom).

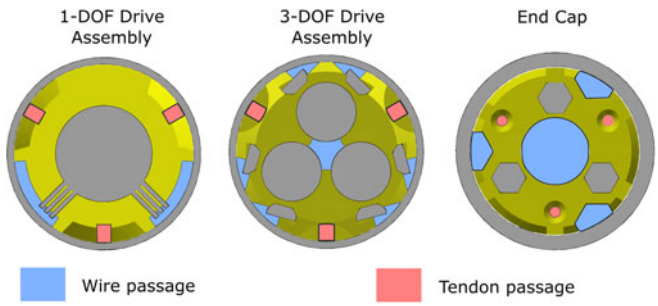

Fig. 3. Front view of the two drive assemblies and end cap showing where wires and working channels could be passed through. The yellow area represents housing which could easily be redesigned to accommodate more wires or working channels. The grey areas represent critical components which are more challenging to redesign.

The outer diameter of all of the collars is 26 mm. The maximum outer diameter of the mesh when uncompressed is approximately 31 mm and 35 mm when compressed. Given that the mesh is a soft material, these diameters are of less concern compared to that of the rigid collar/drive assemblies. As the colon is around 26 mm in diameter at its narrowest [16], however, the device's diameter will need to be reduced in future design iterations. Significant diameter reductions can be achieved by redesigning the sensing system (see Section III-B).

B. Locomotion Strategy

The proposed locomotion strategy (see Fig. 4) takes advantage of the end segments' ability to bend in order to selectively increase frictional forces between the colon wall and the skin of the robot. As it is assumed that the device will always be travelling in a tubular environment, bending one segment to a sufficiently large angle will "jam" it into place. As the tip of the

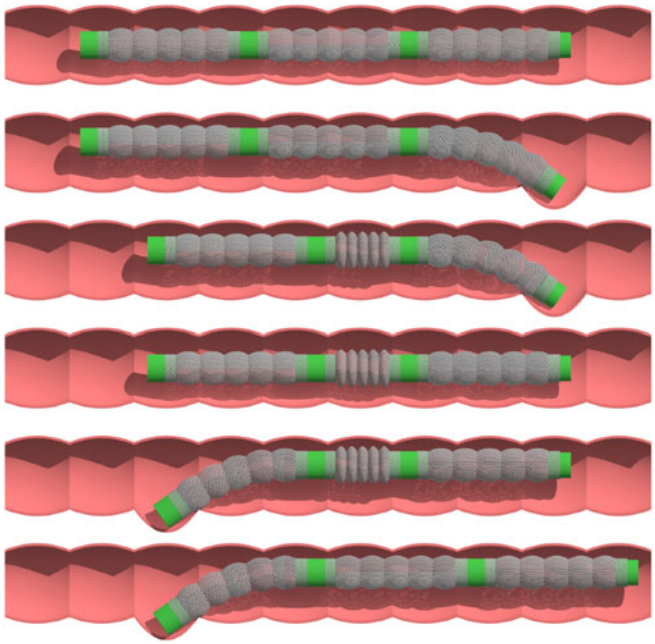

Fig. 4. Illustration of a single iteration of the proposed locomotion sequence.

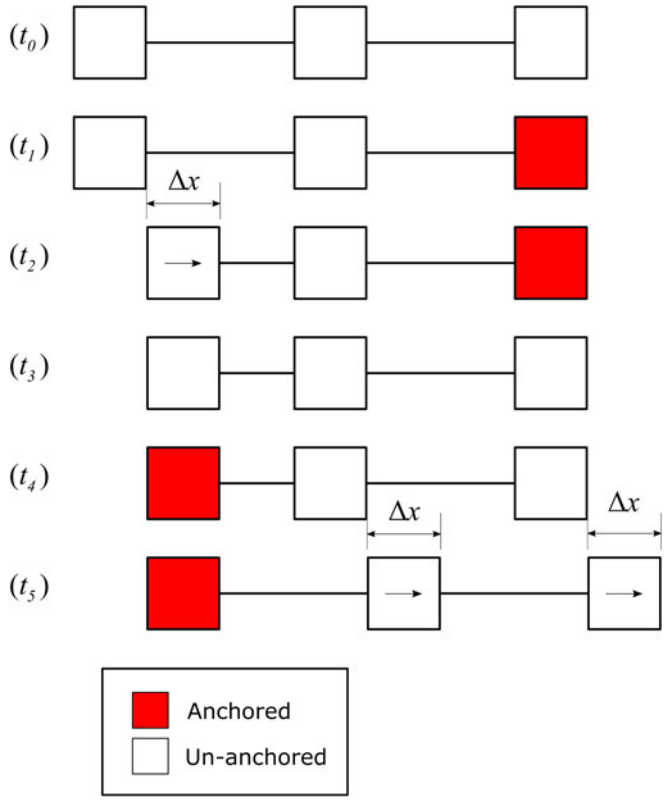

Fig. 5. Simplified diagram of the locomotion sequence.

bending segment presses against one side of the colonic wall, the curved middle section of the segment is pressed against the opposite wall. As the mesh is compliant, it will deform, avoiding damaging the colon and increasing the friction between the colonic wall and the bent segment, thus anchoring it into place. A primary advantage of this method is that the bending angle of the segment can be adjusted to adapt to changing colon diameters. As the diameter of the human colon varies significantly depending on location in the colon [16], this adaptability is highly useful for endoscopy.

Forward motion is achieved by having only one of the end segments anchored. The middle segment is then able to move the unanchored end segment relative to the anchor by contracting or extending. Thus, when done in the correct sequence, forward or backward locomotion may be achieved. Additionally, as each of the end segments can bend, they are able to actively steer the device around turns and control the orientation of a camera mounted on the end. Given that the human colon can be highly tortuous [16], this ability to steer is critical.

C. Locomotion Analysis

In each iteration of the proposed locomotion sequence, the theoretical distance by which the tip of the robot will advance is equal to the contraction distance of the middle segment $\Delta x_{e,\text{ideal}}$. This is illustrated in Fig. 5. Additionally, the total time taken for each iteration is equal to Δt_{tot}. Hence, the ideal speed of the robot may be expressed as

$$v_{\text{ideal}} = \frac{\Delta x_{e,\text{ideal}}}{\Delta t_{\text{tot}}}. \tag{1}$$

From (1), it is clear that to increase speed either $\Delta x_{e,\text{ideal}}$ must be increased or Δt_{tot} must be decreased. While simply making each segment move as fast as possible would increase the speed, modifications to the sequence itself could also potentially improve performance. The sequence shown in Fig. 5 only permits a single segment to move at any given time. By allowing segments to move simultaneously, stages of the original sequence may be skipped, and thus decrease Δt_{tot}. This is achieved by combining stages of the basic sequence so that segments move simultaneously. For example, if the anchoring and unanchoring stages were performed simultaneously for the two end segments, then only four stages would be required, as opposed to six. In other words, the stages at t_0 and t_3 are removed. This is shown in Fig. 6.

In order to have a clearer understanding of how the device performs, the efficiency of locomotion may be defined as

$$\eta_{\text{loc}} = \frac{v_{\text{real}}}{v_{\text{ideal}}} \tag{2}$$

where η_{loc} is the locomotive efficiency and v_{real} is the measured speed of the device. There are two primary ways in which locomotive efficiency could drop, as illustrated in Fig. 6. Firstly, the middle segment could fail to extend completely due to external friction. Since it is not possible to directly control the extension of the mesh (it is only possible to "allow" it to passively extend), this middle segment may not extend completely during operation. Secondly, the anchoring force could be insufficient on one of the end segments and result in an anchored segment slipping. Thus, it is possible to define the actual distance moved forward each iteration Δx_f as

$$\Delta x_f = \Delta x_e - \Delta x_s \tag{3}$$

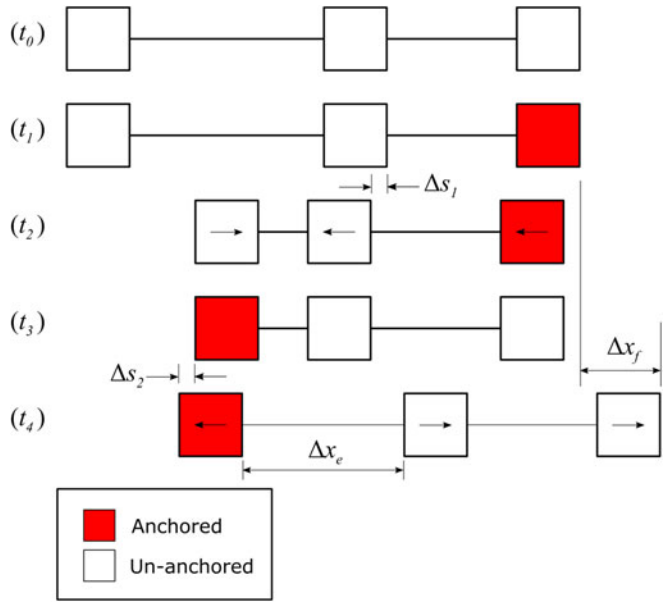

Fig. 6. Diagram of a single iteration of the improved locomotion sequence where non-idealities occur. Δs_i refers to the distance slipped by and Δx_e denotes the actual extension distance of the middle segment.

where $\Delta x_s = \Delta s_1 + \Delta s_2$. The real velocity may then be defined as

$$v_{\text{real}} = \frac{\Delta x_e - \Delta x_s}{\Delta t_{\text{tot}}} = \frac{\Delta x_f}{\Delta t_{\text{tot}}}. \tag{4}$$

With this, additional locomotive efficiencies may be defined in order to better understand the behaviour of the device. Substituting (1) and (4) into (2) yields

$$\eta_{\text{loc}} = \frac{\Delta x_f}{\Delta x_{e,\text{ideal}}} = \frac{\Delta x_e}{\Delta x_{e,\text{ideal}}} \cdot \frac{\Delta x_f}{\Delta x_e} = \eta_e \eta_a \tag{5}$$

where $\eta_e = \frac{\Delta x_e}{\Delta x_{e,\text{ideal}}}$ and $\eta_a = \frac{\Delta x_f}{\Delta x_e}$. The expansion efficiency η_e measures how much of the theoretical expansion is achieved. The anchoring efficiency η_a measures how effectively the system is able to anchor during the locomotion sequence. Thus, two separate quantities can be measured to evaluate the two primary performance aspects of the device.

D. Sequence Implementation

In order to easily implement the locomotion sequence, it is useful to split each sequence into two separate parts: anchoring/unanchoring and contraction/extension. It is reasonable to assume that each individual part will always take the same time to perform. Also, regardless of the details of the locomotion sequence, there will necessarily have to be a contraction stage and an extension stage for the middle segment in order to produce forward movement. Hence, (1) may be rewritten as

$$v_{\text{ideal}} = \frac{\Delta x_{e,\text{ideal}}}{N_{\text{anch}} \Delta t_{\text{anch}} + 2\Delta t_{\text{con}}} \tag{6}$$

where N_{anch} refers to the number of anchoring/unanchoring stages present in the sequence, Δt_{anch} refers to the time taken for a single anchoring/unanchoring stage and Δt_{con} refers to the time taken for a single contraction/extension stage. In (6), only N_{anch} is dependent on the design of the locomotion sequence itself. The variables $\Delta x_{e,\text{ideal}}$, Δt_{con} and Δt_{anch} are dependent on the limitations of the actuators and hardware used in the device. Therefore, N_{anch} is the defining variable which may identify a given locomotion sequence. In this case, $N_{\text{anch}} = 2$.

TABLE I
SUMMARY OF RELEVANT MOTOR PROPERTIES

Property	Motor	
	3-DOF	1-DOF
Rated Voltage / V	3	3
Diameter / mm	6	12
Length / mm	24.0	20.8
Rated Torque / mN-m	10	40
Rated Speed / rpm	37	22
Pulley Radius / mm	2	5
Rated segment contraction speed / mm/s	7.75	11.5
Rated segment contraction distance / mm	67	36

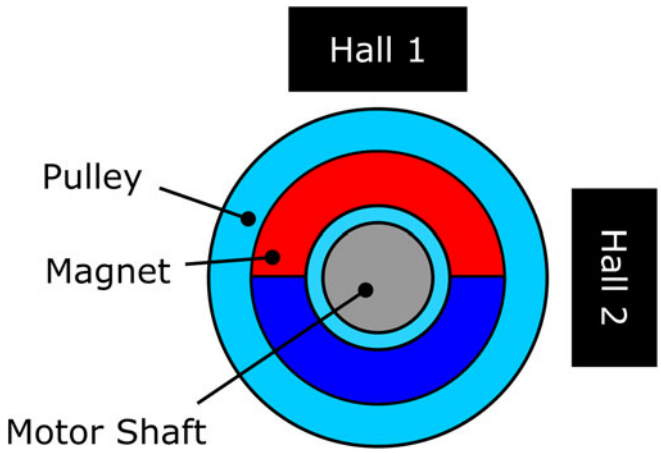

Fig. 7. View of underside of a pulley to illustrate the sensing system's functionality.

III. DESIGN FEATURES

A. Actuator Selection

Miniature DC motors were selected to actuate the robot due to their wide availability and low cost. The Precision Microdrives 206-10C was selected to drive the 3-DOF segment and the larger Precision Microdrives 212-103 12mm DC motor was chosen for the 1-DOF segment. The relevant properties of these motors are summarised in Table I.

With these values, the parameters of the locomotion sequence were selected as follows: $\Delta x_{e,\text{ideal}} = 45\,\text{mm}$, $\Delta t_{\text{anch}} = 3\,\text{s}$ and $\Delta t_{\text{con}} = 4\,\text{s}$.

B. Sensing

In order to implement feedback control on each tendon, a Hall Effect-based sensor system was used. The principle is shown in Fig. 7. A ring-shaped magnet, diametrically magnetized, was

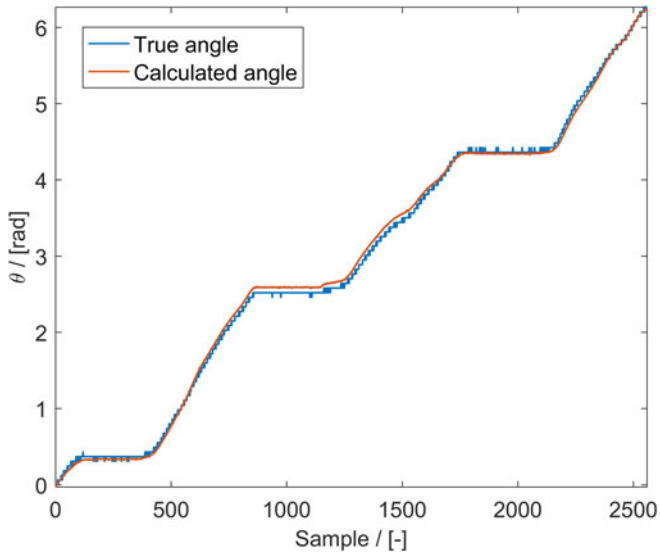

Fig. 8. Plot of a comparison between the angle measured with the potentiometer (the "True angle") and the angle measured with the Hall Effect sensing system ("Calculated angle").

embedded in the bottom of each pulley. Two Hall Effect sensors were placed 90° apart around the perimeter of the pulley. The signal of each sensor varied sinusoidally with the pulley's angular position. As the two sensors were physically 90° apart, the sinusoidal sensor signals were also 90° out of phase. After linearly mapping the two signals such that they each had a value in the range [1, 1], the angle of the pulley could be computed using

$$\theta(t) = \mathrm{Atan2}\left[h_1(t), h_2(t)\right] \tag{7}$$

where $h_1(t)$ and $h_2(t)$ are the Hall Effect sensor readings after mapping. With the absolute angle of the pulley known at any time, it was possible to calculate the length of each tendon with knowledge of some initial tendon length and the associated pulley angle:

$$L(t) = L(0) + \left[\theta(t) - \theta(0)\right] \cdot r_{\mathrm{pulley}}. \tag{8}$$

To evaluate the sensing system, a potentiometer was rigidly attached to a pulley to provide a reliable measurement of the pulley angle. A comparison between the two readings is shown in Fig. 8.

C. Control

A simple PID controller was chosen to control the length of each tendon. This was implemented on a single microcontroller (MCU) board which would process the signals from the Hall Effect sensors in each segment and compute the PID control output. A secondary path planning MCU would compute high level path control information and send this to the other MCU via I^2C bus. This is shown in Fig. 9.

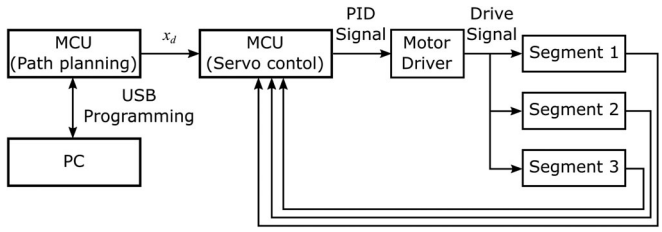

Fig. 9. Block diagram of the control system implemented.

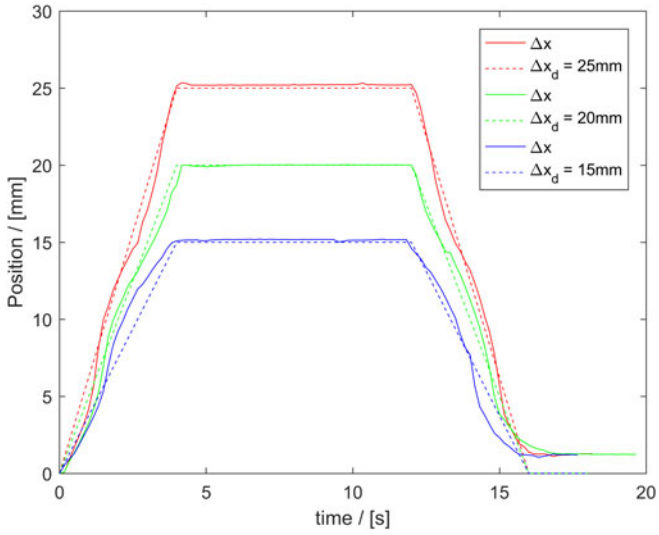

Fig. 10. Step response of the middle section for various contraction distances. The dashed lines indicate the demanded path while the solid lines indicate the actual position of the end of the segment.

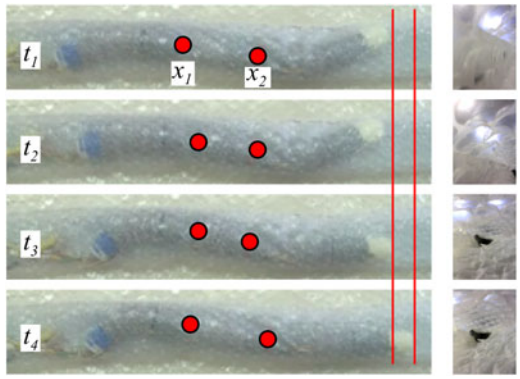

Fig. 11. A time-lapse series of the chosen locomotion squence. The positions of the markers are indicated as red dots. A corresponding view from the on-board camera can be found to the right of each picture.

IV. Experiment

Two experiments were carried out. Firstly, the middle segment step response was evaluated to investigate the effectiveness of the contraction/extension movement. Secondly, the prototype was run through a simulated colon.

A. Step Response

In order to ensure that the middle segment was accurately contracting, a simple step response test was carried out on the

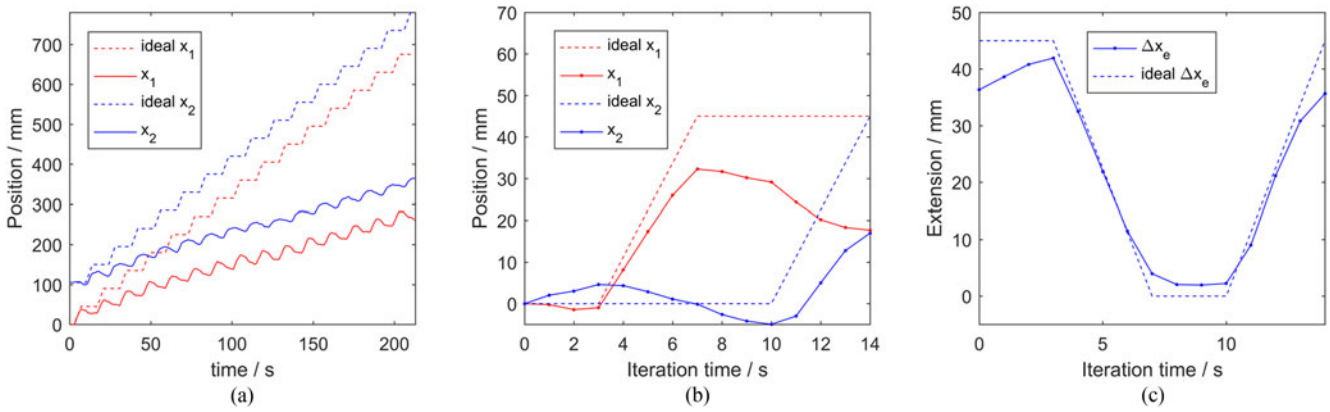

Fig. 12. Results of the locomotion test in the simulated colon. (a) Plot of the middle and rear segment positions over the whole experiment in comparison to their theoretical positions. (b) The average position of the middle segment during one sequence iteration. For simplicity, the results were normalised in order to show that the middle segment always starts at zero. (c) The average extension of the middle segment over a single sequence iteration.

fully assembled prototype. This involved commanding the central segment to contract from an un-extended state to a given new length and then back to its original length. A vision system was used to evaluate the true position of a marker on the end of the central segment.

The results of this are shown in Fig. 10. It is clear from this that the system shows some problems with regard to tracking a dynamic path. The system is, however, sufficiently accurate in reaching the final target position. Upon extending back to its original length, on the other hand, the segment does not reach its original position. This is most likely due to the low restoring forces present at low extensions which are insufficient to overcome friction.

B. Simulated Colon

A sheet of flexible plastic "bubble wrapping" was rolled into a tube to create a simulated colon. This was selected as an appropriate experimental simulacrum primarily due to its soft and compliant properties. The tube was approximately 50 mm in diameter and 1200 mm long. Its internal surface was dry and smooth. The tube was laid on a bench on top of a number of additional layers of bubble wrapping. In order to better account for the fact that the colon is only partially hung and is therefore mobile in the abdominal cavity, only one end of the tube was fixed to the table, while the other was allowed to move freely. The robot would start a run at the free end of the tube and move toward the fixed end.

The bending angles of the two end segments were chosen by trial and error while testing in the simulated colon. It was found that with all segments straight and extended, the robot was subject to around 1.1 N of static frictional force. With the front segment bent, this frictional force increased to around 2.0 N, thus validating that the segment jamming strategy could work in a real colon.

A time-lapse sequence of a single iteration of the locomotion sequence is shown in Fig. 11. The position of two markers on the body of the worm were used to calculate the locomotion parameters discussed in Section II. A plot of the position of the rear and front points of the middle segment (x_1 and x_2 respectively) is shown in Fig. 12(a).

TABLE II
AVERAGE LOCOMOTION TEST RESULTS

$v_{\mathrm{real}}/\mathrm{mm/s}$	$\Delta x_f/\mathrm{mm}$	$\Delta x_e/\mathrm{mm}$	$\Delta x_s/\mathrm{mm}$	η_{loc}	η_e	η_a
1.21	16.99	39.70	22.71	0.38	0.88	0.43

The average speed of the device was calculated by measuring the total distance travelled and the total time taken for the worm to reach its final position. This then allowed η_{loc} to be calculated with knowledge of the ideal speed discussed previously.

The raw data was then separated to allow for each iteration to be analysed individually. Data from each individual iteration was then compared at fixed 1 s intervals. With this data, it was possible to produce an average trajectory for a given marker during a single iteration. These results may be seen in Fig. 12(b) and (c).

The extension at each iteration was calculated by noting the initial distance between x_1 and x_2, denoted as ΔL_0. Then, for each iteration, the total extension for each iteration was calculated according to

$$\Delta x_e = x_2\left(t_4\right) - x_1\left(t_3\right) - \Delta L_0 + \Delta x_{e,\mathrm{ideal}} \tag{9}$$

where $t_3 = 10\,\mathrm{s}$ and $t_4 = 14\,\mathrm{s}$ relative to the beginning of each iteration respectively. Also, $\Delta x_{e,\mathrm{ideal}}$ was added such that when the segment had contracted, a value of zero would be obtained and if a full extension occurred, a value equal to $\Delta x_{e,\mathrm{ideal}}$ would be obtained. The results of the analysis on the average trajectories are shown in Table II.

V. DISCUSSION & CONCLUSION

The prototype performed reasonably well overall. With the average speed of 1.21 mm/s found in the experiment, the device would be able to move from one end of the average human colon with a length of 1850 mm [16] to the other in under 30 min (or just under an hour in order to complete both forward and return journeys). This is consistent with the existing technology of flexible endoscopy, which entails approximately 45 min for an entire procedure [17], but with the advantage of potentially less

pain, if no pain at all – even without sedation, which is required during standard flexible colonoscopy.

The extension efficiency was reasonably high. Looking between $t = 10\,\mathrm{s}$ and $t = 14\,\mathrm{s}$ in Fig. 12(c), the segment is able to extend most of its desired length, but as the compressive energy is reduced, external friction begins to play a larger role and slows down the rate of extension. Therefore, it is not able to complete the full extension during the allocated 4 s.

As a result, during the first anchoring/unanchoring stage of each sequence, some extension would occur in addition to that which had happened during the previous sequence. This can be seen from $t = 0\,\mathrm{s}$ to 3 s in Fig. 12(b) and (c). It can also be seen in Fig. 12(b) that this unintended extension would allow for some forward motion for x_2, but also some backward motion for x_1, as neither end segments are fully anchored during this period. In order to ensure that the extension only occur within the allocated time frame, using a stiffer mesh for the central segment would mean that more compressive force would be available to overcome external friction.

Slipping was observed as occurring on both of the end segments while they were anchored. To mend this, larger bending angles could be employed or the surface qualities of the mesh could be altered to increase grip while bending. Future work could examine the tribological interaction between the robot and the environment to further optimise the robot's performance.

An experiment was carried out to evaluate the device's ability to turn. Due to the limited torque available from the motors used in the 3-DOF segments, a maximum bending angle of 90° was available. It was found that the robot was able to navigate a bend when set at approximately 70°. Beyond this, friction becomes too great. It is therefore reasonable to conclude that the tip must be able to bend at an angle *greater* than the largest angle expected to be encountered. A critical improvement of the design would be to allow the front segment to bend 180°. This can be achieved by sourcing more powerful actuators.

With regard to the design of the robot itself, a number of issues must be addressed in the next iteration of the design. The device must be miniaturised and working channels for air and water must be incorporated. Additionally, the maximum diameter of the colon in which the device can anchor is primarily a function of the length of the two end segments. Therefore, more investigation is required to determine the ideal lengths required for each segment.

Regarding the simulated colon, some of the key properties of the colon were replicated: it was collapsed, partially hung and compliant. The elasticity of colon tissue, however, is significantly greater than the material used in the experiment [18]. It is expected that in order to tackle these challenges, the interaction between each of the 3-DOF segments and the colon wall during anchoring must be examined in detail. This will allow for an optimised anchoring system and will be the topic of future research.

In future, a control interface will also be required. A control interface will be developed as the full details of the locomotion sequence are established.

In conclusion, a novel design for a robotic mesh worm was presented for use in colonoscopy. The device employs a novel new anchoring technique which allows the device to achieve forward locomotion, camera orientation and anchoring with only a single mechanism. A theoretical framework through which to understand the locomotive performance of the device was established. The device was fabricated and tested in a simulated colon, achieving an average speed of 1.21 mm/s. In the future, the theoretical framework will utilised to identify design improvements which will allow the device to be more efficient and achieve higher velocities.

REFERENCES

[1] F. Stracci, M. Zorzi, and G. Grazzini, "Colorectal cancer screening: Tests, strategies, and perspectives," *Frontiers Public Health*., vol. 2, pp. 1–9, Oct. 2014.

[2] P. Valdastri, M. Simi, and R. J. Webster, "Advanced technologies for gastrointestinal endoscopy," *Annu. Rev. Biomed. Eng.*, vol. 14, no. 1, pp. 397–429, 2012.

[3] E. V. Mangan, D. A. Kingsley, R. D. Quinn, and H. J. Chiel, "Development of a peristaltic endoscope," in *Proc. IEEE Int. Conf. Robot. Autom.*, May 2002, pp. 347–352.

[4] A. Menciassi, S. Gorini, G. Pernorio, and P. Dario, "A SMA actuated artificial earthworm," in *Proc. IEEE Int. Conf. Robot. Autom.*, 2004, vol. 4, pp. 3282–3287.

[5] A. Menciassi, D. Accoto, S. Gorini, and P. Dario, "Development of a biomimetic miniature robotic crawler," *Auton. Robots*., vol. 21, no. 2, pp. 155–163, 2006.

[6] W. Lin, Y. Shi, Z. Jia, and G. Yan, "Design of a wireless anchoring and extending micro robot system for gastrointestinal tract," *The Int. J. Med. Robot. Comput. Assisted Surgery: MRCAS*., vol. 9, pp. 167–179, 2013.

[7] K. Wang, G. Yan, P. Jiang, and D. Ye, "A wireless robotic endoscope for gastrointestine," *IEEE Trans. Robot.*, vol. 24, no. 1, pp. 206–210, Feb. 2008.

[8] S. Seok *et al.*, "Meshworm: A peristaltic soft robot with antagonistic nickel titanium coil actuators," *IEEE/ASME Trans. Mechatronics*, vol. 18, no. 5, pp. 1485–1497, Oct. 2013.

[9] J. Pfeffer *et al.*, "The Aer-O-Scope: Proof of the concept of a pneumatic, skill-independent, self-propelling, self-navigating colonoscope in a pig model," *Endoscopy*, vol. 38, no. 2, pp. 144–148, 2006.

[10] T. Rösch *et al.*, "A motor-driven single-use colonoscope controlled with a hand-held device: a feasibility study in volunteers," *Gastrointestinal Endoscopy*, vol. 67, no. 7, pp. 1139–1146, 2008.

[11] S. Groth, D. K. Rex, T. Rösch, and N. Hoepffner, "High cecal intubation rates with a new computer-assisted colonoscope: A feasibility study," *The Am. J. Gastroenterol.*, vol. 106, no. 6, pp. 1075–1080, 2011.

[12] A. Eickhoff *et al.*, "In vitro evaluation of forces exerted by a new computer-assisted colonoscope (the NeoGuide Endoscopy System)," *Endoscopy*., vol. 38, no. 12, pp. 1224–1229, 2006.

[13] A. Eickhoff *et al.*, "Computer-assisted colonoscopy (The neoguide endoscopy system): Results of the first human clinical trial ('PACE study')," *American J. Gastroenterol.*, vol. 102, no. 2, pp. 261–266, 2007.

[14] F. Cosentino, E. Tumino, G. R. Passoni, E. Morandi, and A. Capria "Functional evaluation of the Endotics System, a new disposable self-propelled robotic colonoscope olIn vitro tests and clinical trial," *Int. J. Artif. Organs*, vol. 32, no. 8, pp. 517–527, 2009.

[15] T. Manwell, T. Vítek, T. Ranzani, A. Menciassi, K. Althoefer, and H. Liu, "Elastic mesh braided worm robot for locomotive endoscopy," in *Proc. 36th Annu. Int. Conf. IEEE Eng. Med. Biol. Soc.*, 2014, pp. 848–851.

[16] A. Alazmani, A. Hood, D. Jayne, A. Neville, and P. Culmer, "Quantitative assessment of colorectal morphology: Implications for robotic colonoscopy," *Med. Eng. Phys.*, vol. 38, no. 2, pp. 148–154, 2016.

[17] P. B. Cotton *et al.*, "Colonoscopy: Practice variation among 69 hospital-based endoscopists," *Gastrointestinal Endoscopy*, vol. 57, no. 3, pp. 352–357, 2003.

[18] C. Stefanini, A. Menciassi, and P. Dario, "Modeling and experiments on a legged microrobot locomoting in a tubular, compliant and slippery environment," *The Int. J. Robot. Res.*, vol. 25, nos. 5/6, pp. 551–560, 2006.